Three Dimensional Iterative Scouring Methodology Using Commercial CFD Software

(Preliminary results – stay tuned for coming model enhancements)

Offshore Center Denmark [1] conducted several experiments by varying the flow velocities and also provided a numerical model using FLUENT and compared the results. The results are limited to a very small (0.25mm) sediment size. The experimental setup consisted of a long rectangular flume with a cylinder in the center representing the wind turbine structure. The experiment was limited to cases where turbine supports were placed in ocean settings. Guo et. al [2] analytically determined the average bed and sidewall shear stresses for steady uniform flow in smooth rectangular channels. Their formulations show the importance of three main terms in the shear stress analysis: (1) a gravitational term; (2) a secondary flow term; and (3) a shear stress term at the interface. Van Rijn [3] experimentally determined sediment pick-up rate by using sediment lift installed in the center of the experimental flume. The sediment pick-up rate formula determined by him is used in the present study. In the previous phase of this project, Elapolu [4] developed a 3-D iterative methodology using existing commercial CFD software STAR-CCM+ to estimate a scour hole profile around bridge piers by moving the sediment boundary downward proportional to the supercritical shear stress. Results were compared to experiment data from Offshore Center Denmark. Simulations were limited to cases of a circular bridge pier and the critical shear stress at any point did not account for the slope of the bed. Guo [5] determined an approximate relation for the shear stress. His relation compares well with experimental results. His approximation is used in this study due to its simplicity.

Pier Scour Simulation Setup and Meshing

Simulations are run using STAR-CCM+ version 5.04.008. The simulations are implicit unsteady using a varying time step and employ the standard k-epsilon turbulence model along with wall function treatment. A half flume is modeled by placing a symmetry plane along the center of the flume, running in the direction of flow, to save computational time. The computational domain can be seen in Figure 4.1. It extends from -2 m to +2 m in the primary flow or X-direction, 0.6 m to 0 m in the cross stream or Z-direction, and 0 m to 0.17 m in the vertical or Y-direction. The domain is divided into two regions along the height of the cylinder in order to ensure that mesh morphing occurs only on the bottom region to save computational time and prevent a previously encountered problem of negative volume cells being generated at the top surface after morphing.

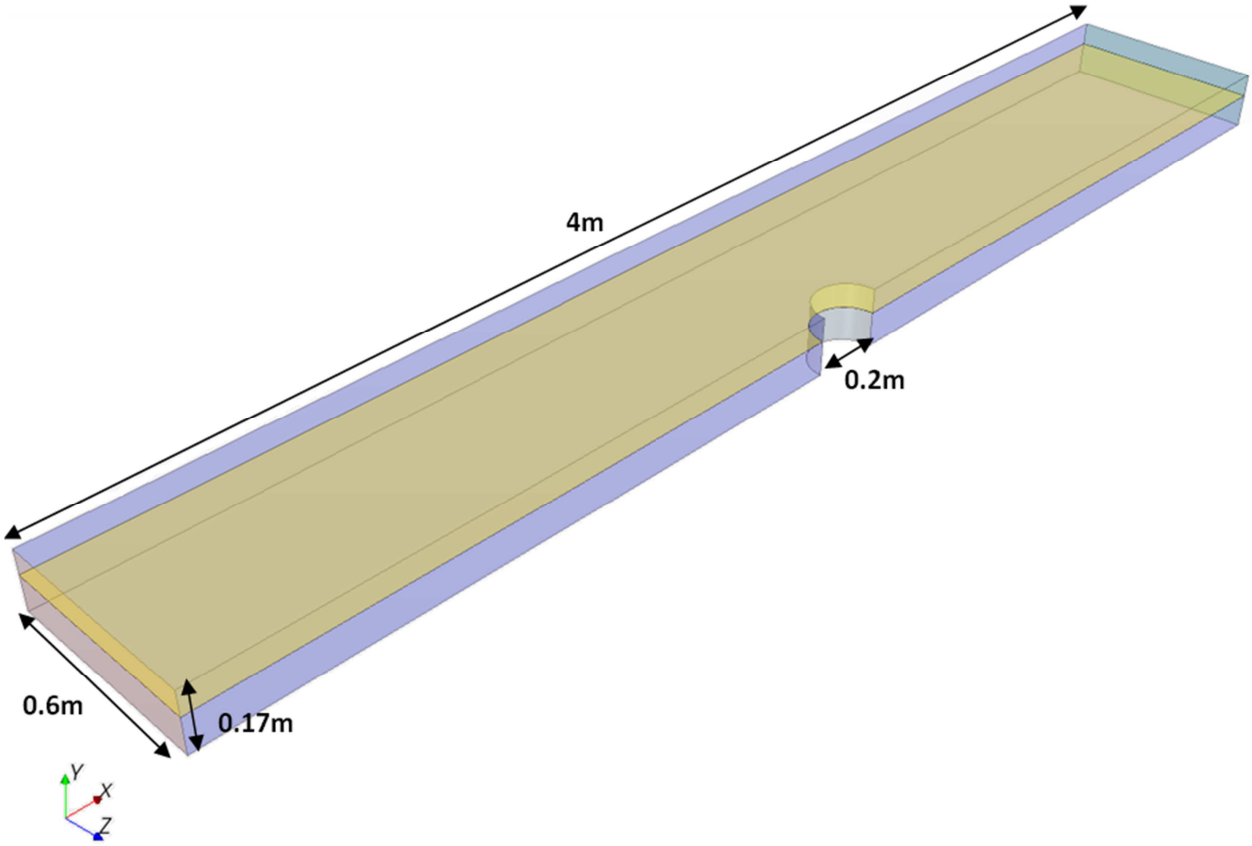

Figure 4.1: Computational domain with dimensions and key lengths

The computational domain is meshed using a core cell size of 20mm. A refined mesh is placed around the bridge pier and a prism layer is used at the bed boundary and pier wall to maintain the correct cell thickness for the application of turbulent wall functions (satisfying the y+ y^+wall requirement). 8mm is specified as the near wall prism layer thickness. A cell size of 5 mm was used to refine the grid around the cylindrical pier, as shown in Figure 4.2 that provides details of a zoomed isometric view of the mesh around the cylindrical pier.

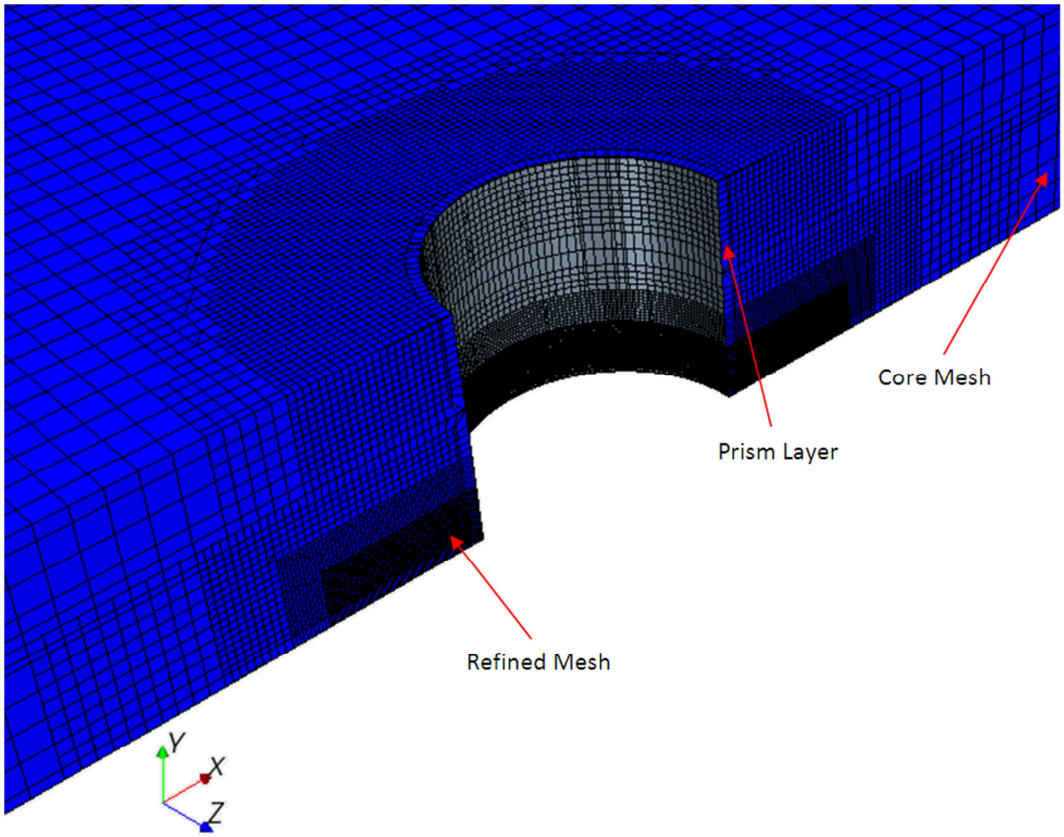

Figure 4.2: Isometric view of mesh around cylindrical bridge pier

The boundaries of the computational domain have different parameters. A list of each boundary along with its associated boundary condition in the computational domain and boundary condition for mesh morphing is given in Table 4.1. The inlet has a specified inlet velocity with magnitude of 0.5m/s as well as turbulent kinetic energy and turbulent dissipation rate of 0.0025 m^2/s^2 and 0.004 m^2/s^3, respectively.

Table 4.1: Boundary conditions of the computational domain

Boundary	Boundary Condition	Morphing Condition
Inlet	Velocity Inlet	Fixed
Outlet	Flow-Split Outlet	Fixed
Bed	Wall	Grid Velocity
Front	Symmetry	N/A
Back	Wall	Fixed
Top	Symmetry	N/A
Interface	Interface	Fixed
Cylinder Top	Wall	N/A
Cylinder Bottom	Wall	Floating

Mesh Morphing

The means to simulate scour hole formation is done through a mesh morphing model in STAR-CCM+. After every time step the bed boundary is displaced with a grid velocity calculated by means of a user defined field function that takes into account the local supercritical shear stress. Then the bed moves downward, but the mesh morphing does not stretch just the layer of cells adjacent to the bed boundary, rather it distributes stretching of the cells throughout a chosen region in order to maintain a high quality mesh. If the morphed mesh cells become overly stretched due to the formation of very deep scour holes, the situation is remedied by remeshing the domain part way through the computation.

Scouring Relation and Time Step Formulation

The methodology in this study involves moving the initial flat bed downwards in small increments proportional to the supercritical shear stress at a point on the bed. This downward motion is only in the vertical, or y-direction. A grid velocity is used to actually move the bed boundary in each time step. The grid velocity with which the bed has to be moved in the downward direction is calculated using a derivation of Van Rijn's experimentally determined entrainment rate function given as

$$\frac{dh}{dt} = \frac{0.00033\sqrt{\Delta g d_{50}}d_*^{0.3}}{\theta_s}\left(\frac{\tau_{bed}}{\tau_c} - 1\right)^{1.5} \quad 4.1$$

where

$$\Delta = (\rho_s - \rho)/\rho \quad 4.2$$

$$d_* = d_{50}\left[\frac{\Delta g}{\nu^2}\right]^{1/3} \quad 4.3$$

$$\theta_s = 1 - \gamma \quad 4.4$$

Where ρ_s $\rho_s$and ρρ are the densities of the sediment and the water respectively, $\tau_c\tau_c$ is the critical shear stress related to the average sand diameter [5]. $\tau_{bed}\tau_{bed}$ is the shear stress at a point on the bed, g is the acceleration due to gravity, $d_{50}d_{50}$ is the mean sand diameter, γ is the porosity of the sand, $dh/dt\frac{dh}{dt}$ is the recession velocity of the grid in the vertical direction, and ν is the kinematic viscosity.

Two variations of the grid velocity are used. One uses just Equation 4.1, which is termed constant critical shear stress (CCSS) while the second uses Equation 4.5 to adjust the shear stress at the bed to account for the slope of the bed in shear stress calculations, termed variable critical shear stress (VCSS), seen below.

$$\tau_{sloped} = \frac{\sin(\alpha + \phi)}{\sin(\phi)} \tau_{flat\ bed} \quad 4.5$$

Where α is the angle between the sloped bed normal vector and the flat bed normal vector and ϕ is the angle of repose, taken as 33 degrees. The length of each time step is determined based on the maximum specified bed displacement and grid velocity, given by the following equation

$$\Delta t = \Delta \mathrm{y}_{\max} / \frac{dh}{dt} \quad 4.6$$

where Δy_{max} is the user specified maximum displacement for each time step and Δt is the length of each time step. In the following results a maximum displacement of 0.25mm is used. The maximum displacement per time step has been chosen such that it does not cause numerical instability. The scour bed displacement per time step is obtained by the following relation

$$\Delta y = \frac{dh}{dt} \Delta t \quad 4.7$$

is applied to displace each point on the bed where the shear stress exceeds critical at the conclusion of each time step. Mesh morphing after every time step propagates the bed displacements through the volume mesh. The mesh velocity that arises from the mesh morphing is included in the momentum and other transport equations, and therefore conservation law cell balances are maintained with the mesh morphing operation.

Simulation Results

Found below are simulation results that use a mesh that does not fully capture the bed roughness height. Prism layers for the results below are 5mm, which would give an effective bed roughness height of 2.5 mm which is 1.125 times the average sand diameter. In practice, effective roughness heights would be 2 times the average sand diameter. Simulations with effective roughness heights are currently being run and those results will be presented at the next opportunity.

Figure 4.3 shows the scour hole formation using the variable critical shear stress (VCSS) and a constant critical shear stress (CCSS) approach, respectively. The scour hole is elongated in the wake region in Figure 4.3 (a), and has a more defined scour hole upstream of the cylinder. The scour hole is smoother and has steeper side walls in the VCSS approach than predicted by the CCSS approach. Steep side walls are not found in limited experimental results. Also, the maximum scour depth is larger and more area is scoured deeper using the VCSS approach. Red and blue areas represent no scour and deepest scour, respectively.

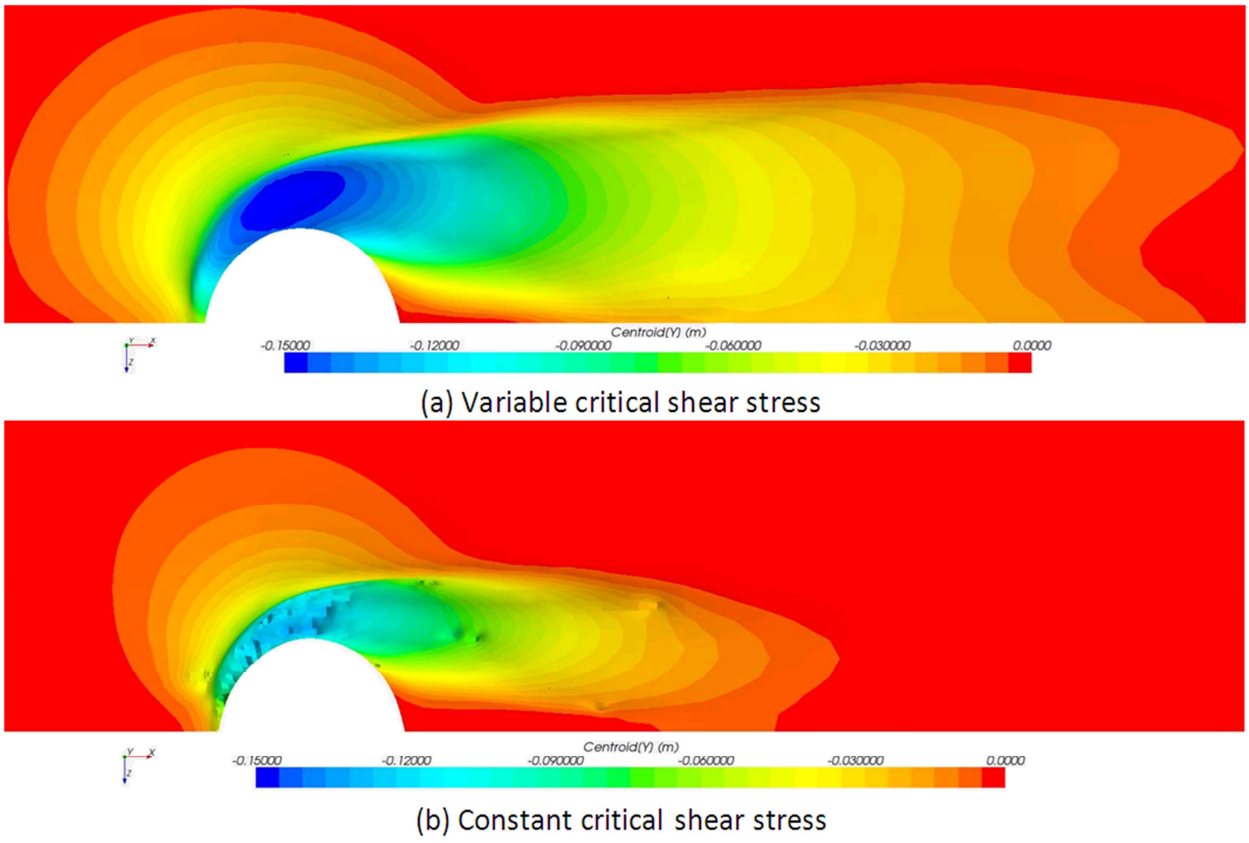

Figure 4.3: Comparison of scoured bed contour at equilibrium using variable and constant critical shear stress

Figure 4.4 shows the evolution of the bed shear stress as it progresses from flat bed to equilibrium based on VCSS and CCSS approaches, respectively. Scouring begins after 10 seconds of simulation time; this allows a quasi-steady state condition to be established that is physically realistic before starting the transient computation. The VCSS case took approximately 50% longer in simulation time to reach equilibrium scour depth, but both cases ran in approximately the same clock time before equilibrium was achieved. The jaggedness in the curves are a consequence of remeshing, which does not preserve cell wall fluxes and property balances due to interpolation error in translating the solution to the new mesh. Use of the variable critical shear stress appears to yield a smoother evolution of the shear stress under the remeshing operation.

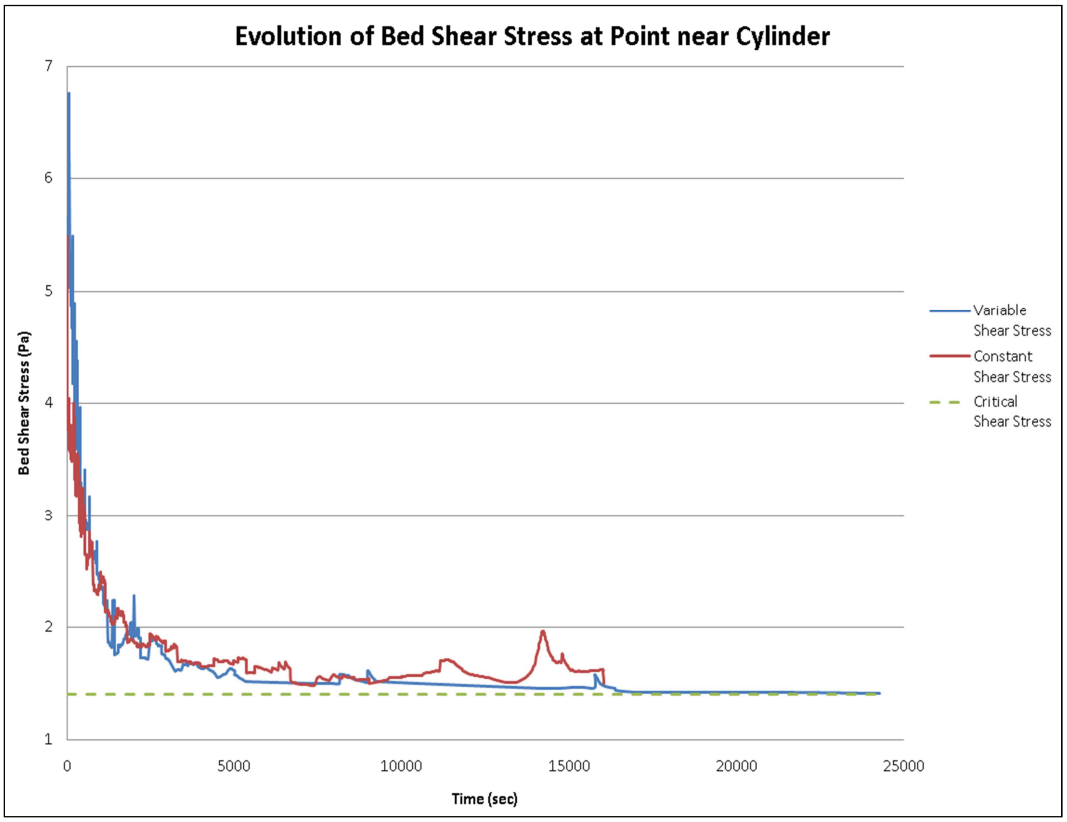

Figure 4.4: Evolution of bed shear stress at a point near the pier (0,0,-0.1025)

Figure 4.5 shows the bed shear stress at equilibrium using VCSS and CCSS approaches. The smallest shear stress value shown is 1.41 Pa, which corresponds to the pre-determined critical shear stress. There are still cells where shear stress is above the critical value, but the stopping criteria is taken at a point located at (0, 0,-0.1025) where the shear stress is below critical. There is still some very slow scouring occurring in the wake region of both cases, but nothing that would adjust the overall look of the scour hole or increase the maximum scour depth. Therefore, for all practical purposes, both cases have come to equilibrium.

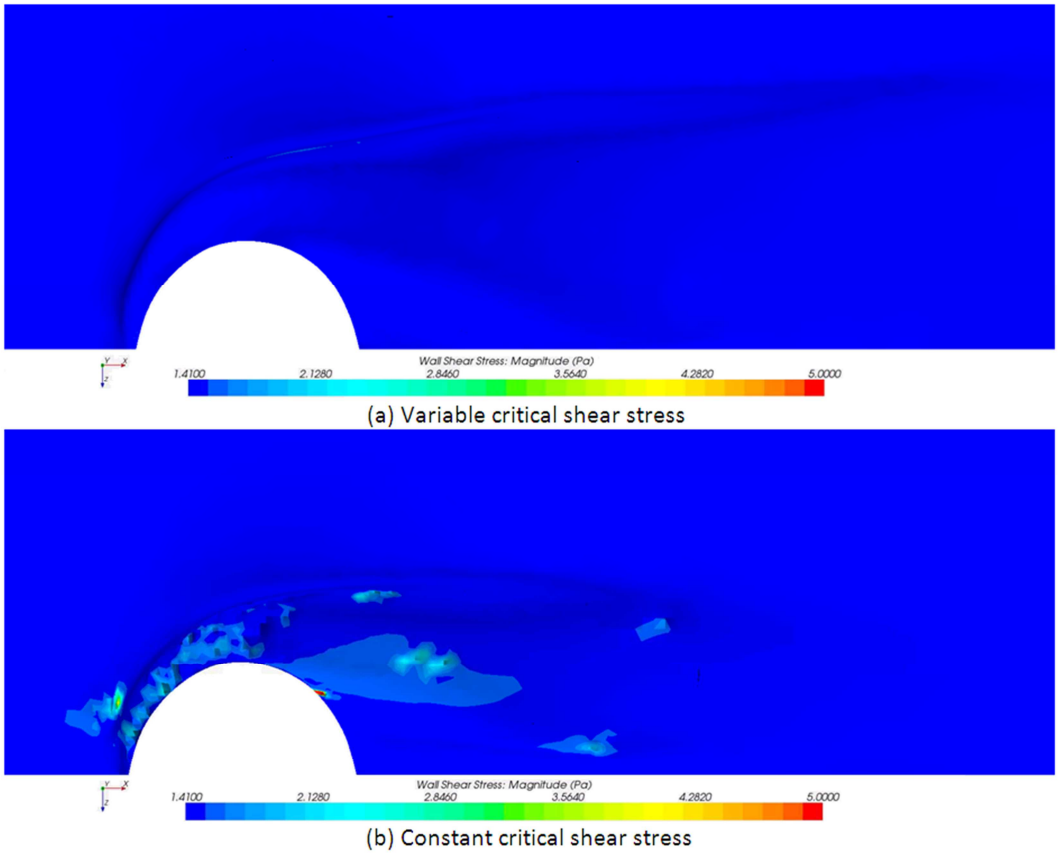

Figure 4.5: Final bed shear stress at equilibrium using constant and variable critical shear stress

References

1. Offshore Center Denmark. "Experimental Study of Scour around Offshore Wind Turbines in Areas with Strong Currents." 2006.

2. Guo, Junke and Julien, Pierre Y. "Shear Stress in Smooth Rectangular Open-Channel Flows," Journal of Hydraulic Engineering © ASCE / January 2005, 30-37.

3. Leo C. van Rijn, "Sediment Pick-Up Functions", Journal of Hydraulic, Vol.110, No. 10, October 1984, pp.1494-1502.

4. Elapolu, Phani (2010). "Development of a Three-Dimensional Iterative Methodology using a Commercial CFD Code for Flow Scouring around Bridge Piers." M.S. Thesis. Department of Mechanical Engineering, Northern Illinois University.

5. Guo, Junke (2002). Hunter Rouse and Shields Diagram. Advances in Hydraulic and Water Engineering, Vol. 2, pages 1096-1098.